

## Research Article

# Layered double hydroxide nanozyme decorated polycaprolactone membranes as superoxide radical scavengers

Adel Szerlauth<sup>a</sup>, Shivesh Anand<sup>b</sup>, Imre Szenti<sup>c</sup>, Menglin Chen<sup>b</sup>, Mingdong Dong<sup>d</sup>, Zoltán Kónya<sup>c</sup>, István Szilágyi<sup>a,\*</sup>

<sup>a</sup> MTA-SZTE Momentum Biocolloids Resarch Group, Department of Physical Chemistry and Materials Science, University of Szeged, Szeged H-6720, Hungary

<sup>b</sup> Department of Biological and Chemical Engineering, Aarhus University, Aarhus DK-8000, Denmark

<sup>c</sup> Department of Applied and Environmental Chemistry, University of Szeged, Szeged H-6720, Hungary

<sup>d</sup> Interdisciplinary Nanoscience Center, Aarhus University, Aarhus DK-8000, Denmark

## ARTICLE INFO

## Keywords:

Clay  
 Enzyme mimic  
 PCL  
 Antioxidant  
 Formulation

## ABSTRACT

The excess amount of reactive oxygen species (ROS) is a crucial problem in health and in many industrial processes. Nanozymes of antioxidant enzyme mimicking features are promising ROS scavengers, however, their formulation is challenging. This work focuses on the development of a ROS decomposing polymer mesh by immobilization of Cu(II) containing layered double hydroxide (CMA3) nanozymes on the surface of polycaprolactone (PCL) membranes prepared by the electrospinning method. The CMA3 nanoparticles were electrosprayed on PCL meshes resulting in the formation of nanozyme ring patterns. The amount of immobilized CMA3 was proportional to the flow rate during electrospraying, while the interfacial spider web-like structure was not significantly affected by this parameter. The obtained PCL-CMA3 composite materials showed remarkable superoxide radical anion scavenging activity. Such a decoration of the PCL mesh with CMA3 provides a possible solution for antioxidant nanozyme formulation for biomedical and industrial applications combatting the overproduction of ROS molecules.

## 1. Introduction

Reactive oxygen species (ROS), like superoxide radical anions, hydroxyl radicals, singlet oxygen and hydrogen peroxide play an important role in various redox reactions that cause harmful oxidative modifications in biological macromolecules (e.g., proteins, nucleic acids and lipids) [1]. On the other hand, ROS are indispensable in certain physiological processes including cell signaling, immune responses and redox regulations [2]. Thus, their level must be precisely balanced by the antioxidant defense system [3]. In case of external or internal perturbation of this delicate equilibrium, illnesses such as cancer [4], inflammation [5] and cardiovascular diseases [6] may develop. Moreover, the increased concentration of ROS is responsible for various skin diseases (e.g., atopic dermatitis and diabetic wounds) and inefficient tissue regeneration processes [7]. Above a certain level, they can inhibit the healing process and cause severe pain and discomfort to patients. In addition to the undesirable physiological effects, elevated ROS level is a major problem in the industry too. In food manufacturing, for instance, prevention of oxidation (e.g., meat, fruit and dairy products) by ROS molecules is a considerable challenge [8].

Due to the above reasons, supplementation of natural and/or artificial antioxidants attracts widespread contemporary attention [9–13]. For example, nanozymes has recently surfaced as possible alternative to native molecular and enzymatic antioxidants, as they have similar biocatalytic functions accompanied by more advantageous properties (e.g., operating in wide range of pH, temperature and pressure, while well dispersible in water) compared to the natural counterparts [14]. They can be divided into two groups, such as nanoparticles with immobilized antioxidants (type I) and nanoparticles with intrinsic enzyme-like activity (type 2) [10]. Oxidase [15], catalase (CAT) [16], superoxide dismutase (SOD) [17] or peroxidase [18] activity of inorganic nanoparticles (ceria [19], Au [20], Fe<sub>3</sub>O<sub>2</sub> [21] and layered double hydroxide (LDH) [22]) were reported in the past.

Concerning LDHs, they are one of the most studied groups of clay minerals, both in terms of surface and structural modification [23,24], and applications as nanozymes are receiving growing interest [18,22,25–27]. Immobilization of biomolecules in/on LDH nanoparticles (type I nanozyme) was comprehensively investigated [28–30], while other studies focused on the structural modification (type II nanozyme) based on the adjustable metal ion composition. For the lat-

\* Corresponding author.

E-mail address: [szistvan@chem.u-szeged.hu](mailto:szistvan@chem.u-szeged.hu) (I. Szilágyi).

ter, Mn [18], Ru [26], Fe [22], Co [27] and Cu [25] doped MgAl-LDHs of single or multi-enzymatic antioxidant functions have been synthesized. Despite of the great efforts in development of LDH-based nanozyme systems, practical applications are still hindered by various factors, for instance, proper formulation for skin treatments or packaging materials.

In this way, polymer meshes are promising platforms to formulate nanoparticles by immobilization in/on the fibers [31]. Electrospinning is a common method for the production of polymer membranes of well-distributed structure that can be prepared from many natural macromolecules (e.g., polycaprolactone (PCL), polyvinyl alcohol, chitosan or gelatin) [8]. The electrospun polymeric scaffold has a similar architecture to the fibrillary structure of the extracellular matrix, which can be beneficial for biomedical applications [32], while its advantageous mechanical properties and structural tuneability promote the use in active food packaging [33].

PCL is a popular precursor material in electrospinning due to its biocompatibility, moderate biodegradability and low cost [34–36]. Many examples are known in the literature, in which PCL has been used as a host for the immobilization of natural antioxidants and/or antimicrobial compounds [8]. Accordingly, PCL membranes containing melanin [37], chlorogenic acid [38], green tea [33] and oregano essential oil [39] have already been developed for active food packaging to prevent the ROS-induced food spoilage. In addition, curcumin [40], tannic acid [41], taxifolin [42], vitamin C [43], pomegranate peel extract [44] and lignin [45] have been incorporated into PCL to improve wound healing, post-operative adhesion and to treat osteoarthritis.

Although the immobilization of natural antioxidants has been widely studied, their research in the solution/dispersion phase is increasingly overshadowed by the growing interest in type II nanozymes [10]. This trend is due to the fact that nanozymes perform better than natural antioxidants in certain properties (e.g., easier and cost-effective preparation, stability). Therefore, there is an urgent need to investigate immobilized nanozymes from various aspects. While natural antioxidants have been widely studied in PCL-based systems, there is a lack of comprehensive investigation involving the immobilization of nanozymes on PCL membranes. Only a few recent studies could be found, which can be summarized as follows. Accordingly, curcumin has already proven as a promising material for wound healing applications and its combination with metal nanoparticles also showed advantageous properties [46]. The PCL scaffolds containing curcuminoid and metal nanoparticles showed great radical scavenging ability separately, but the highest activity was observed once they were applied together. In addition to its antioxidant property, the scaffold also showed antimicrobial activity, making it a promising material for biomedical applications. As an example of type II nanozymes, ceria nanoparticles were immobilized in PCL/gelatine nanofibers and conferred excellent superoxide scavenging activity to the scaffold resulting in enhanced cell growth on the membrane surface and thus, promoting wound healing [47]. Besides, Cu modified carbonitride particles were embedded into PCL membranes giving rise to broad spectrum antibacterial activity on various multidrug resistant bacteria as well as to anti-inflammatory effects [48]. To the best of our knowledge, no data have been published with electrospun fibers consisting of LDH-based antioxidant nanozymes and PCL matrix.

Therefore, the aim of this work was to develop a novel nanozyme-loaded PCL membrane that can be used in certain biomedical or industrial applications. The Cu(II)-loaded LDH nanoparticles (CMA3) were immobilized on the as-synthesized PCL membranes by the electro spray method (Scheme 1). The formation of the PCL/CMA3 hybrid was confirmed by various structural characterization methods, while its SOD-like activity was determined in chemical test reaction. With the superb antioxidant activity, PCL/CMA3 membranes pave the way for application of polymer-nanozyme materials in wound dressings or in active food packaging.

## 2. Experimental section

### 2.1. Materials

Copper chloride dihydrate ( $\text{CuCl}_2 \cdot 2\text{H}_2\text{O}$ ), magnesium chloride hexahydrate ( $\text{MgCl}_2 \cdot 6\text{H}_2\text{O}$ ), aluminium chloride hexahydrate ( $\text{AlCl}_3 \cdot 6\text{H}_2\text{O}$ ), sodium hydroxide pellet (NaOH), xanthine and nitro blue tetrazolium (NBT) were purchased from VWR International, while polycaprolactone (PCL) ( $M_w = 80000$ ), dichloromethane (DCM), dimethyl formamide (DMF) and xanthine oxidase were acquired from Sigma Aldrich. The materials were used without any further purification.

### 2.2. Synthesis of CMA3 particles

The CMA3 nanozymes were synthesized according to our previously established protocol [25]. In brief, 0.12 mol/L  $\text{CuCl}_2 \cdot 2\text{H}_2\text{O}$ , 0.48 mol/L  $\text{MgCl}_2 \cdot 6\text{H}_2\text{O}$  and 0.2 mol/L  $\text{AlCl}_3 \cdot 6\text{H}_2\text{O}$  were dissolved in 5 mL ultrapure water and mixed with 20 mL NaOH solution (0.4 mol/L). After 40 min of stirring, the dispersion was centrifuged and washed 2 times (4200 rpm, 10 min). The slurry was redispersed in 20 mL ultrapure water, transferred to an autoclave and treated at 100 °C overnight. Finally, the sample was centrifuged (4200 rpm, 5 min) and the supernatant was used for further measurements.

### 2.3. Fabrication of PCL membranes

PCL (12 w/v%) was dissolved in a DCM/DMF (3:2) mixture under vigorous stirring overnight. A voltage of 10 kV and a flow rate of 2 mL/h were used for electrospinning to produce the meshes. Electrospinning was run for 2 h while the distance between the needle and the collector was set to 12 cm and the collector was rotated at 1100 rpm. The meshes were then dried overnight.

### 2.4. Immobilization of CMA3 nanoparticles on the PCL meshes

CMA3 samples (1000 mg/L) were immobilized on PCL meshes using the electro spray method. Accordingly, the dispersion was sprayed onto the membrane at 15 kV voltage and a flow rate in the range of 0.625–10 mL/h. The distance between needle and collector was set to 12 cm and the collector was rotated at 1100 rpm for 30 min. The meshes containing CMA3 are referred to as PCL/CMA3/ $x$  ( $x = 0.625, 1.25, 2.5, 5$  and 10 mL/h).

### 2.5. Morphological characterization

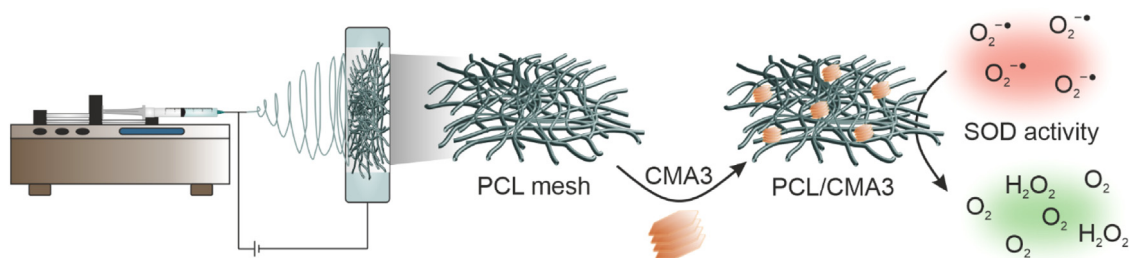
A Hitachi TM3030 Plus benchtop scanning electron microscope with an accelerating voltage of 15 kV was used to study the morphological properties of PCL membranes and CMA3 modified PCL membranes (PCL/CMA3). The PCL and PCL/CMA3 meshes were fixed to the sample holder with a double-sided carbon adhesive tape.

### 2.6. Scanning electron microscopy coupled energy dispersive X-ray spectroscopy (SEM-EDX)

The elemental composition was analyzed using a Thermo Fisher Scientific Apreo C SEM operating at a current of 40 nA and an accelerating voltage of 20 kV.

### 2.7. Structural characterization

A Bruker Senterra II Raman microscope was used to record Raman spectra of PCL and modified PCL membranes. The spectra were collected by using a light source of 532 nm wavelength and 25 mW laser power. Final data were obtained by averaging 32 spectra with an exposition time of 4 s. UV-VIS spectra of diffuse reflectance (DRS) were recorded



**Scheme 1.** Schematic representation of the preparation and SOD-like activity of the PCL/CMA3 composite developed.

with a SHIMADZU UV-3600i Plus UV-VIS-NIR-DRS spectrophotometer. The instrument is equipped with PMT, InGaAs, and PBs detectors. The spectra were measured in 200–450 nm range with 0.1 nm resolution.

X-ray diffractograms were recorded with a Rigaku XRD-Miniflex II instrument operating with  $\text{CuK}\alpha$  radiation ( $\alpha = 0.15418$  nm). The diffractograms were recorded in the  $2\theta$  range of 3–80°, with a scan speed of 2°/min, using 40 kV accelerating voltage at 30 mA.

### 2.8. Enzymatic activity test

The enzymatic activity of the samples was determined using the Fridovich assay [49]. This test can be used to determine the SOD activity of the samples. During the reaction of xanthine and xanthine oxidase, superoxide radical ions are formed, which can reduce the NBT dye, while the reaction mixture turns purple. To test the activity of the immobilized CMA3 samples, 1 cm<sup>2</sup> circles were cut from the meshes. Then, 20  $\mu\text{L}$  xanthine (3 mM), 50  $\mu\text{L}$  NBT (3 mM), 30  $\mu\text{L}$  xanthine oxidase (3 g/L) and 240  $\mu\text{L}$  ultrapure water were mixed, while the PCL/CMA3 mesh was immersed in the reaction mixture. The absorbance was measured (at 565 nm wavelength) before and after 6 min from the start of the reaction and the differences ( $\Delta A$ ) were calculated. The SOD-like activity was expressed in terms of inhibition of the NBT-superoxide radical reaction as follows:

$$\text{Inhibition (\%)} = \frac{\Delta A_0 - \Delta A_s}{\Delta A_0} \times 100\%, \quad (1)$$

where  $A_0$  is the absorbance without, while  $A_s$  is the absorbance with the PCL/CMA3 meshes. The absorbance values of the reaction mixtures were recorded with a Genesys™ 10S UV-VIS spectrophotometer.

## 3. Results and discussion

### 3.1. Development of PCL/CMA3 composite fibers

To produce ROS scavenging membranes, a polymer scaffold made of PCL was first produced by electrospinning. As shown in Fig. 1(a), the PCL fibers were randomly oriented and the average diameter of the fibers was determined to be  $0.583 \pm 0.258$   $\mu\text{m}$  (Fig. 1(b)). The polymer meshes were then used to immobilize the CMA3 samples on their surface.

The characterization of CMA3 nanoparticles was reported elsewhere [25]. Briefly, the MgAl-LDH structure was modified by isomorphous substitution to partially replace Mg(II) with Cu(II) ions to confer antioxidant activity to the nanoparticles. The incorporation of the Cu(II) ions and the formation of lamellar structure was confirmed with various experimental techniques. The nanoparticles exhibited remarkable SOD and CAT activity in standard chemical tests and successfully reduced intracellular oxidative stress. Therefore, by deposition of the nanoparticles on the PCL meshes, the development of a highly active antioxidant membrane was foreseen.

The CMA3 samples were immobilized on PCL meshes by the electrospay method, varying the flow rate in the range of 0.625–10 mL/h. The CMA3 nanoparticles were visible on the surface and formed well-defined

**Table 1**

Elemental analysis results (at% means atomic percentage).

Sample	Magnesium (at%)	Copper (at%)
PCL	–	0.01 $\pm$ 0.00
PCL/CMA3/0.625	0.19 $\pm$ 0.10	0.02 $\pm$ 0.01
PCL/CMA3/1.25	0.06 $\pm$ 0.04	0.02 $\pm$ 0.00
PCL/CMA3/2.5	0.27 $\pm$ 0.04	0.02 $\pm$ 0.01
PCL/CMA3/5	2.26 $\pm$ 0.58	0.11 $\pm$ 0.04
PCL/CMA3/10	4.36 $\pm$ 1.30	0.26 $\pm$ 0.14

ring-shaped motifs (Figs. 2(a)–(g)). The ring-shaped motifs are related to the so-called coffee-ring phenomenon. Since PCL is hydrophobic, the aqueous dispersion of CMA3 was deposited in droplets on the PCL meshes during the electrospay method (Fig. 2(a)(1)). When a droplet contains colloidal particles, the evaporation of the solvent can trigger a capillary flow mechanism. Namely, the solvent evaporating from the edge is replaced by the flow of solvent carrying the particles to the edge of the droplet (Fig. 2(a)(2)), forming a coffee-ring-shaped deposition (Fig. 2(a)(3)) [50,51]. At the highest flow rate (10 mL/h), the speed is high enough to cause the coalescence of the droplets on the surface, and the loss of the ring-shaped structure. The schematic representation of the formation of the coffee-ring structure is shown in Fig. 2(a).

At low flow rates, CMA3 initially formed slightly elongated rings, whereas with a further increase (1.25–5 mL/h), the CMA3 rings exhibited a more regular shape, while at 10 mL/h it disappeared and a more flooded morphology appeared. The diameter of the rings initially decreased with increasing the flow rate, while above 2.5 mL/h, a higher ring diameter was measured (see the 5 mL/h data in Fig. 2(e)). At 10 mL/h, the ring diameter could no longer be determined as the ring-shaped motifs on the surface disappeared. At higher magnification, it became visible at the edge of the rings that the CMA3 nanoparticles formed a spider web-like structure, i.e., the nanozyme samples completely covered the adjacent PCL fibers (Fig. S1 in the Supplementary material). It was found that the appearance of the spider web-like morphology was independent of the flow rates, i.e., the morphology at the edge of the rings was very similar in each case.

Besides, the membranes were subjected to elemental analysis to determine the CMA3 content. The EDX results revealed that the Mg(II) and Cu(II) concentrations increased (i.e., more CMA3 was immobilized) at higher flow rates (Table 1). Note that the Cu(II) level was close to the detection limit of the instrument, however, the Mg(II) content clearly demonstrated the presence of CMA3 nanoparticles on the PCL surface.

Results of UV-VIS-DRS measurements also confirmed the immobilization of CMA3 nanoparticles on the PCL membranes. The CMA3 nanozymes showed an intense absorption peak at 223 nm wavelength. However, at low flow rates (1.25 mL/h and below) an intense absorption band appeared in the 280–330 nm range (pink shadow in Fig. 3(a)) for the CMA3 modified PCL membranes.

This band is assigned to the charge transfer processes [52] associated with the interactions between the polymer membrane and the CMA3 nanoparticles. The intensity of this band decreases with increasing CMA3 concentration, which is due to the fact that the amount of

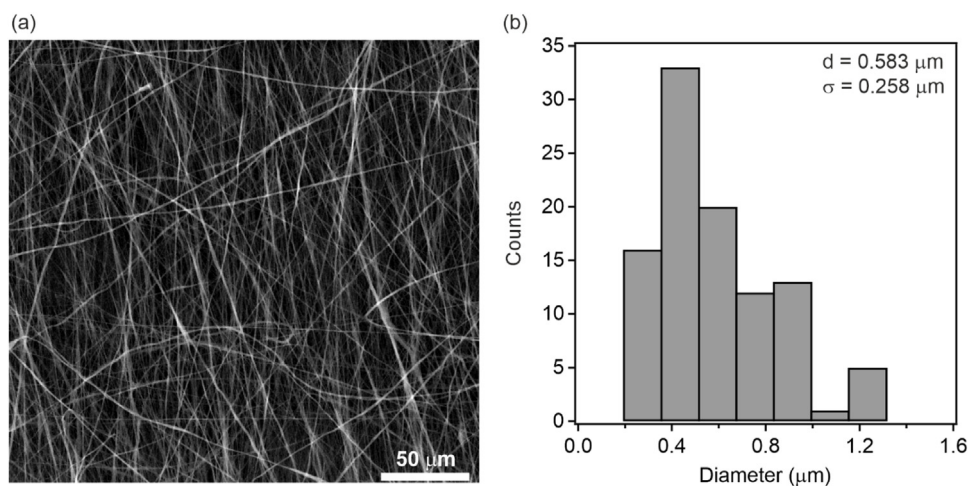


Fig. 1. SEM image (a) and the size distribution (b) of PCL fibers width. The average diameter ( $d$ ) and the standard deviation ( $s$ ) are in the inset of (b).

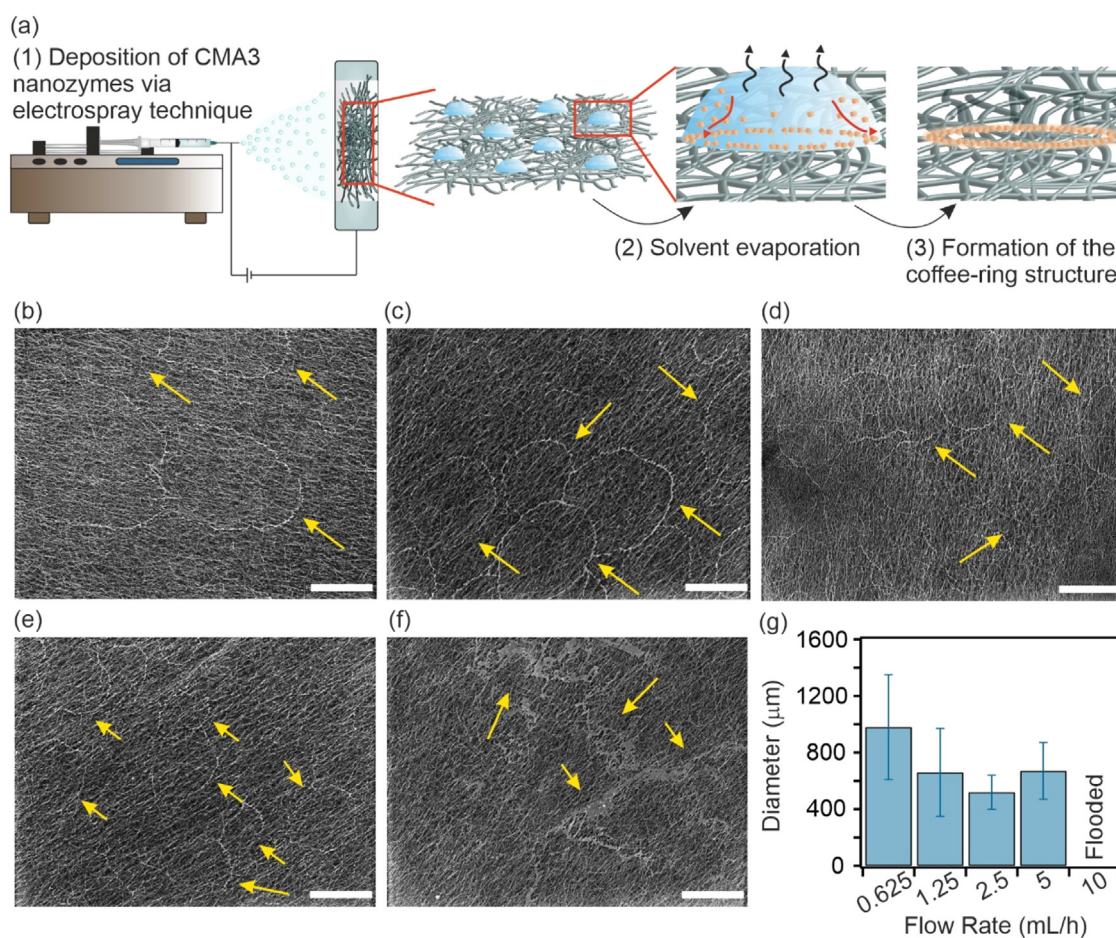


Fig. 2. Schematic representation of the coffee-ring effect that occurs after electro-spraying CMA3 onto PCL membranes (a). Black arrows represent the evaporation, while red arrows show the capillary flow of the solvent. SEM image of CMA3 modified PCL meshes using 0.625 mL/h (b), 1.25 mL/h (c), 2.5 mL/h (d), 5 mL/h (e) and 10 mL/h (f) flow rate during preparation. The change in ring diameter as a function of the applied flow rates (g). The yellow arrows on the SEM images label the CMA3 rings formed after electro-spraying the dispersion on the PCL meshes. The scale bars represent 500 μm.

adsorbed CMA3 particles increases and therefore, more particle aggregates can form on the PCL surface. This has already been confirmed by the SEM results, where a flooded morphology of the samples appeared at higher flow rates. In line with the decreasing intensity of the charge transfer band, the peak associated with the absorption band of CMA3 shifted towards the position of the one recorded for the pristine

nanoparticles (grey shadow in Fig. 3(a)). This is also consistent with the above mentioned theory. As the concentration of CMA3 increased and consequently, the interaction between the nanozymes strengthened, the band related to the nanoparticles appeared closer to its original position. Thus, the location and intensity of these bands clearly confirmed the immobilization of CMA3 nanoparticles on the PCL surface and also

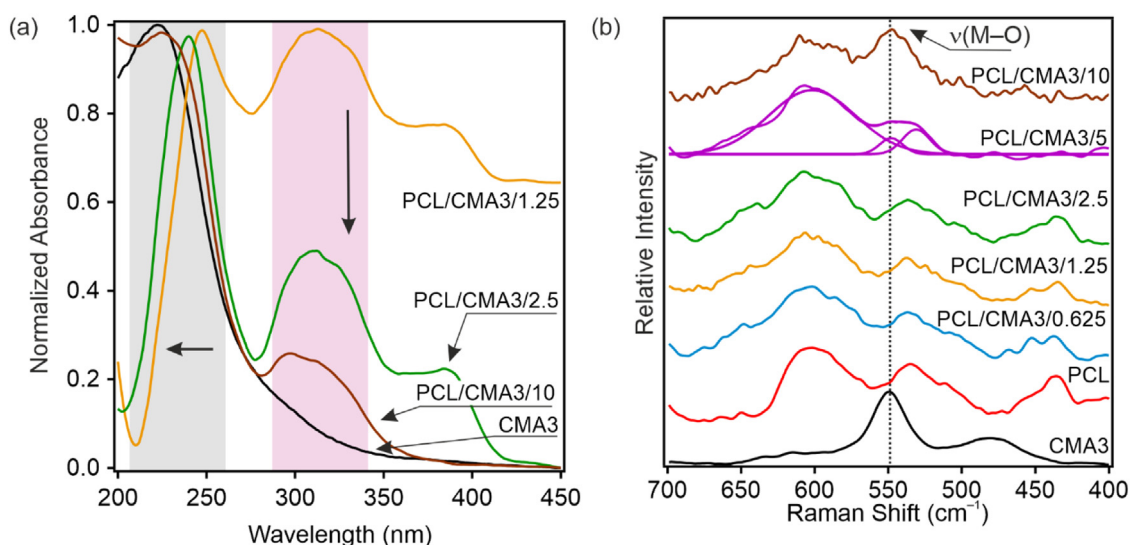


Fig. 3. UV-VIS (a) and Raman (b) spectra of CMA3, PCL and the modified PCL membranes. The spectra are labelled with their name on each graph.

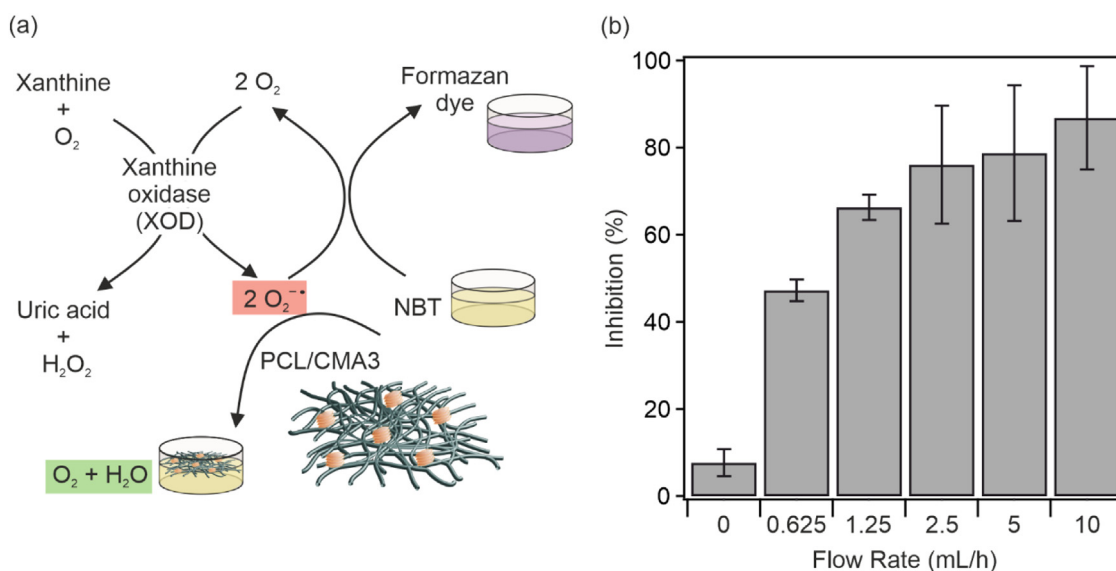


Fig. 4. Illustration of the SOD-like activity assessment of the PCL/CMA3 samples (a) and the NBT-superoxide radical reaction inhibition data determined (b).

give information about the adsorption mechanism of the nanozymes. The UV-VIS spectra of PCL/CMA3/0.625 and PCL/CMA3/5 are shown in Fig. S2.

The Raman microscopy results also proved the presence of CMA3 nanoparticles on the PCL mesh (Fig. 3(b)). The Raman band at  $550\text{ cm}^{-1}$  associated with the  $\nu(\text{M-O})$  vibration appeared in the spectra of PCL/CMA3/10 and PCL/CMA3/5, while no characteristic peak of the nanozyme appeared in at lower flow rates, i.e., the Raman bands in these spectra originated from the PCL membrane. The absence of the band associated with CMA3 in the range of 0.625–5 mL/h flow rates can be explained by the low concentration of the nanoparticles present in the composite samples.

Finally, to investigate the crystal structure of PCL membranes and to further confirm the presence of CMA3 nanozymes, XRD measurements were also performed on bare PCL, PCL/CMA3/5 and PCL/CMA3/10 (Fig. S3). The reflections of PCL appeared at  $21.8^\circ$  and  $24.0^\circ$   $2\theta$  values in all three samples, which are related to the (110) and (200) planes of the orthorhombic crystal phase of PCL [53,54]. The XRD patterns confirm that immobilization of CMA3 had no effect on the crystal structure of PCL. However, the characteristic reflection of CMA3 also appeared at

$12.3^\circ$   $2\theta$  value, which is related to the (003) Bragg reflection of the LDH nanoparticles [25].

### 3.2. SOD-like activity assessment

The superoxide radical scavenging activity of the CMA3 containing samples was investigated in the Fridovich assay [49]. In a typical test, superoxide radicals are formed during the reaction between xanthine and xanthine oxidase, while they subsequently react with the NBT dye in the solution leading to color change from yellow to blue. If an enzyme or a nanozyme that can dismutate superoxide radicals is present, the reaction between the dye and the radicals is inhibited and hence, no color change occurs [25,28,55]. The measurements were carried out by soaking the CMA3 containing membranes in the reaction mixture. The schematic representation of the reactions taking place during the assay and the color change are illustrated in Fig. 4(a).

PCL without CMA3 nanoparticles was used as control and the data in Fig. 4(b) reveals that no significant inhibition occurred in this case. However, immobilizing the CMA3 nanoparticles imparted SOD-like activity to the matrix and a clear correlation was observed between the

**Table 2**

Maximal inhibition (%) data of native and immobilized SOD, and the bare and immobilized CMA3 nanozyme.

Sample	Maximal inhibition (%)	Reference
SOD	95–100	[28]
dLDHaHtSC	80	[28]
CMA3	90	[25]
PCL/CMA3	80	This work

flow rate and inhibition. Accordingly, increasing the flow rate, i.e., higher amount of CMA3 on the PCL surface, gave rise to an increase in superoxide radical scavenging activity. Immobilizing CMA3 on PCL with 0.625 mL/h flow rate increased the inhibition by ~50% compared to the bare PCL mesh. The 1.25 mL/h condition led to a further increase in inhibition, while above 2.5 mL/h, the activity became nearly constant (~80%). This trend indicates that the inhibition above 2.5 mL/h is independent of the CMA3 concentration, so that the reachable maximum inhibition of the PCL/CMA3 composite sample is ~80%.

For comparison, the maximum inhibition of the native enzyme is over 90%, while 80% was reported for the immobilized SOD (Table 2) [28]. The CMA3 nanozyme resulted in a similar maximum inhibition as the native enzyme, while PCL/CMA3 showed about 80%, which was slightly lower compared to the free (non-immobilized) CMA3. These results imply that a slight reduction of the activity occurred upon immobilization of both the native enzyme on an inorganic host material and the CMA3 nanozyme on the PCL mesh.

It should be noted that the CMA3 nanoparticles possessed CAT activity in the dispersion phase but lost their ability to decompose hydrogen peroxide after immobilization on PCL membranes. The loss of CAT activity can be explained by the reduced concentration of the nanozyme in the reaction mixture. For PCL/CMA3/10, the nanozyme content on the 1 cm<sup>2</sup> PCL membrane is approx. 8 µg, which is too low to detect CAT activity. Most likely, further increasing the CMA3 concentration during preparation or applying a larger area of PCL mesh would increase CAT activity, but due to the limitation of the enzymatic assay, such tests could not be performed. Nevertheless, the developed PCL/CMA3 hybrid materials have great antioxidant potential due to the advanced ability to scavenge superoxide radicals, but it should be noted that the generated hydrogen peroxide may hinder its application, e.g., in wound healing processes. However, further modification with a hydrogen peroxide degrading enzyme (e.g., CAT) or nanozyme (e.g., CeO<sub>2</sub>) may overcome this limitation.

#### 4. Conclusions

In conclusion, CMA3 was successfully immobilized on prefabricated PCL membranes by the electrospray method to obtain SOD mimicking PCL/CMA3 scaffolds. A systematic variation in the flow rates during CMA3 adsorption revealed that they have significant effects on the formation of circle-shaped motives, while no influence on the spider web-like shape within the circles was observed. The presence of CMA3 in the composite was further revealed by determining the elemental composition of the membranes prepared as well as with spectroscopy methods by assigning the characteristic vibrations to the components. The CMA3 retained its SOD-like activity upon immobilization on PCL. In addition, its maximal inhibition was close to the native SOD enzyme. Overall, a CMA3 functionalized PCL scaffold with efficient superoxide radical scavenging activity was developed and it represents a promising candidate in biomedical and industrial applications, in which the local elimination of superoxide radicals (and/or other ROS) is crucial, for instance during wound healing or food packaging.

#### Declaration of Competing Interest

Mingdong Dong is an editorial board member for ChemPhysMater and was not involved in the editorial review or the decision to publish

this article. The authors declare that they have no known competing financial interests or personal relationships that could have appeared to influence the work reported in this paper.

#### CRediT authorship contribution statement

**Adel Szerlauth:** Writing – original draft, Validation, Methodology, Investigation, Data curation. **Shivesh Anand:** Writing – review & editing, Methodology, Formal analysis. **Imre Szentı:** Writing – review & editing, Methodology, Investigation. **Menglin Chen:** Writing – review & editing, Supervision, Conceptualization. **Mingdong Dong:** Writing – review & editing, Validation, Funding acquisition. **Zoltán Kónya:** Writing – review & editing, Resources, Funding acquisition. **István Szilágyi:** Writing – review & editing, Supervision, Project administration, Funding acquisition, Conceptualization.

#### Acknowledgements

This work was supported by the [National Research, Development and Innovation Office \(2024-1.2.3-HU-RIZONT-2024-00035\)](#), the Hungarian Academy of Sciences ([LP2022-16-2022](#)) and the European Union's Horizon Europe research and innovation program under the Marie Skłodowska-Curie Action project ENSIGN ([101086226](#)).

#### Supplementary materials

Supplementary material associated with this article can be found, in the online version, at [doi:10.1016/j.cphma.2025.10.001](https://doi.org/10.1016/j.cphma.2025.10.001).

#### References

- [1] T. Wang, M.R. Bai, W. Geng, M. Adeli, L. Ye, C. Cheng, Bioinspired artificial antioxidantases for efficient redox homeostasis and maxillofacial bone regeneration, *Nat. Commun.* 16 (2025) 856.
- [2] M. Schieber, N.S. Chandel, ROS function in redox signaling and oxidative stress, *Curr. Biol.* 24 (2014) 453–462.
- [3] H. Sies, D.P. Jones, Reactive oxygen species (ROS) as pleiotropic physiological signalling agents, *Nat. Rev. Mol. Cell Biol.* 21 (2020) 363–383.
- [4] S. Reuter, S.C. Gupta, M.M. Chaturvedi, B.B. Aggarwal, Oxidative stress, inflammation, and cancer. How are they linked? *Free Radic. Biol. Med.* 49 (2010) 1603–1616.
- [5] G. Schett, M.F. Neurath, Resolution of chronic inflammatory disease: Universal and tissue-specific concepts, *Nat. Commun.* 9 (2018) 3261.
- [6] M.A. Incalza, R. D'Orta, A. Natalicchio, S. Perrini, L. Laviola, F. Giorgino, Oxidative stress and reactive oxygen species in endothelial dysfunction associated with cardiovascular and metabolic diseases, *Vasc. Pharmacol.* 100 (2018) 1–19.
- [7] L. Zhang, Y.N. Ma, X.C. Pan, S.Y. Chen, H.H. Zhuang, S.F. Wang, A composite hydrogel of chitosan/heparin/poly ( $\gamma$ -glutamic acid) loaded with superoxide dismutase for wound healing, *Carbohydr. Polym.* 180 (2018) 168–174.
- [8] J. Brito, H. Hlushko, A. Abbott, A. Aliakseyeu, R. Hlushko, S.A. Sukhishvili, Integrating antioxidant functionality into polymer materials: Fundamentals, strategies, and applications, *ACS Appl. Mater. Interfaces* 13 (2021) 41372–41395.
- [9] H.M. Zhong, C. Jiang, Y.Y. Huang, The recent development of nanozymes for targeting antibacterial, anticancer and antioxidant applications, *RSC Adv.* 13 (2023) 1539–1550.
- [10] M. Zandieh, J.W. Liu, Nanozymes: definition, activity, and mechanisms, *Adv. Mater.* 36 (2024) 2211041.
- [11] H. Wei, G. Li, J. Li, Biomedical nanozymes: From diagnostics to therapeutics, Springer Nature, Singapore, 2023.
- [12] M. Zandieh, J.W. Liu, Surface science of nanozymes and defining a nanozyme unit, *Langmuir* 38 (2022) 3617–3622.
- [13] R.S.M. Brito, J. Milanesio, M.B. Oviedo, J.M. Padró, M.C. Strumia, F. Mattea, Tannic acid-modified poly(acrylamide-co-acrylic acid): A versatile approach for aqueous viscosity modulation, *ACS Appl. Polym. Mater.* 6 (2024) 4462–4474.
- [14] R.Z. Tian, J.Y. Xu, Q.A. Luo, C.X. Hou, J.Q. Liu, Rational design and biological application of antioxidant nanozymes, *Front. Chem.* 8 (2021) 831.
- [15] Y.X. Xing, L. Li, Y.H. Chen, L. Wang, S.Q. Tang, X.Y. Xie, S. Wang, J.X. Huang, K.Y. Cai, J.X. Zhang, Flower-like nanozyme with highly porous carbon matrix induces robust oxidative storm against drug-resistant cancer, *ACS Nano* 17 (2023) 6731–6744.
- [16] Y.M. Sun, S.D. Mu, Z.Y. Xing, J.S. Guo, Z.H. Wu, F.Y. Yu, M.R. Bai, X.L. Han, C. Cheng, L. Ye, Catalase-mimetic artificial biocatalysts with Ru catalytic centers for ROS elimination and stem-cell protection, *Adv. Mater.* 34 (2022) 2206208.
- [17] N. Lihi, Z. Balogh, R. Dioszegi, A. Forgacs, K. Moldovan, N.V. May, P. Herman, I. Fabian, J. Kalmar, Functionalizing aerogels with tetraazamacrocyclic copper(II) complexes: Nanoenzymes with superoxide dismutase activity, *Appl. Surf. Sci.* 611 (2023) 155622.

- [18] X.T. Yang, X. Cao, Y. Fu, J. Lu, X.T. Ma, R. Li, S.Y. Guan, S.Y. Zhou, X.Z. Qu, Layered double hydroxide-based nanozyme for NO-boost multi-enzyme dynamic therapy with tumor specificity, *J. Mat. Chem. B* 11 (2023) 1591–1598.
- [19] N. Thakur, P. Manna, J. Das, Synthesis and biomedical applications of nanoceria, a redox active nanoparticle, *J. Nanobiotechnol.* 17 (2019) 84.
- [20] Y.H. Lin, J.S. Ren, X.G. Qu, Nano-gold as artificial enzymes: Hidden talents, *Adv. Mater.* 26 (2014) 4200–4217.
- [21] S. Tanaka, M.K. Masud, Y.V. Kaneti, M.J.A. Shiddiky, A. Fatehmulla, A.M. Aldhafiri, W.A. Farooq, Y. Bando, M.S.A. Hossain, Y. Yamauchi, Enhanced peroxidase mimetic activity of porous iron oxide nanoflakes, *ChemNanoMat* 5 (2019) 506–513.
- [22] Y.P. Ning, Y. Sun, X. Yang, Y.P. Li, A.J. Han, B.Q. Wang, J.F. Liu, Defect-rich CoFe-layered double hydroxides as superior peroxidase-like nanozymes for the detection of ascorbic acid, *ACS Appl. Mater. Interfaces* 15 (2023) 26263–26272.
- [23] C. Dazon, C. Taviot-Guého, V. Prévot, Layered double hydroxides: Where should research stress on for massive scaling up? *Mater. Adv.* 4 (2023) 4637–4645.
- [24] T.T. Hu, Z. Gu, G.R. Williams, M. Strimaite, J.J. Zha, Z. Zhou, X.C. Zhang, C.L. Tan, R.Z. Liang, Layered double hydroxide-based nanomaterials for biomedical applications, *Chem. Soc. Rev.* 51 (2022) 6126–6176.
- [25] A. Szerlauth, T. Madácsy, G.F. Samu, P. Bíró, M. Erdélyi, G. Varga, Z.P. Xu, J. Maléth, I. Szilágyi, Reduction of intracellular oxidative stress with a copper-incorporated layered double hydroxide, *Chem. Commun.* 60 (2024) 1325–1328.
- [26] B.Q. Wang, Y.Y. Fang, X. Han, R.T. Jiang, L. Zhao, X. Yang, J. Jin, A.J. Han, J.F. Liu, Atomization-induced high intrinsic activity of a biocompatible MgAl-LDH supported Ru single-atom nanozyme for efficient radicals scavenging, *Angew. Chem. Int. Ed.* 62 (2023) e202307133.
- [27] S. Zhang, J. Chen, W.S. Yang, X. Chen, Vacancies-rich CoAl monolayer layered double hydroxide as efficient superoxide dismutase-like nanozyme, *Nano Res.* 15 (2022) 7940–7950.
- [28] A. Szerlauth, Á. Varga, T. Madácsy, D. Sebők, S. Bashiri, M. Skwarczynski, I. Toth, J. Maléth, I. Szilágyi, Confinement of triple-enzyme-involved antioxidant cascade in two-dimensional nanostructure, *ACS Mater. Lett.* 5 (2023) 565–573.
- [29] M. Pavlovic, A. Szerlauth, S. Muráth, G. Varga, I. Szilágyi, Surface modification of two-dimensional layered double hydroxide nanoparticles with biopolymers for biomedical applications, *Adv. Drug Deliv. Rev.* 191 (2022) 114590.
- [30] L.X. Zhang, J. Hu, Y.B. Jia, R.T. Liu, T. Cai, Z.P. Xu, Two-dimensional layered double hydroxide nanoadjuvant: Recent progress and future direction, *Nanoscale* 13 (2021) 7533–7549.
- [31] W.B. Wang, C.Y. Pan, E.Y. Huang, B.J. Peng, J.A.T. Hsu, J.C. Clapper, Electrospun polyacrylonitrile silver(I,III) oxide nanoparticle nanocomposites as alternative antimicrobial materials, *ACS Omega* 7 (2022) 48173–48183.
- [32] K.M. Kennedy, A. Bhaw-Luximon, D. Jhurry, Cell-matrix mechanical interaction in electrospun polymeric scaffolds for tissue engineering: Implications for scaffold design and performance, *Acta Biomater* 50 (2017) 41–55.
- [33] L.Y. Maroufi, S. PourvatanDoust, F. Naeijian, M. Ghorbani, Fabrication of electrospun polycaprolactone/casein nanofibers containing green tea Essential oils: Applicable for active food packaging, *Food. Bioprocess Technol.* 15 (2022) 2601–2615.
- [34] V. Rahimkhoei, M. Padervand, M. Hedayat, F. Seidi, E.A. Dawi, A. Akbari, Biomedical applications of electrospun polycaprolactone-based carbohydrate polymers: A review, *Int. J. Biol. Macromol.* 253 (2023) 126642.
- [35] T.A. Augusto, M.C. Crovace, L.A. Pinto, L.C. Costa, Polycaprolactone/F18 bioactive glass scaffolds obtained via fused filament fabrication, *ACS Appl. Polym. Mater.* 7 (2025) 2359–2370.
- [36] A. Sarmah, A.J. Zervoudakis, M.R. Pfau-Cloud, M.A. Hillmyer, C.J. Ellison, Chemical recycling of polycaprolactones via reactive melt processing, *ACS Appl. Polym. Mater.* 7 (2025) 1763–1770.
- [37] M. Garcia-Garcia, D. Orona-Tamayo, A. Estrada-Monje, E. Quintana-Rodriguez, R. Navarro-Mendoza, L. Hernandez-Perales, N.E. Lozoya-Perez, J.S. Jaime-Ferrer, Melanin from pecan nut shell waste as an antioxidant and antifungal additive in membranes for food packaging, *J. Polym. Environ.* 33 (2025) 1469–1490.
- [38] Y.C. Zou, C. Zhang, P. Wang, Y.P. Zhang, H. Zhang, Electrospun chitosan/polycaprolactone nanofibers containing chlorogenic acid-loaded halloysite nanotube for active food packaging, *Carbohydr. Polym.* 247 (2020) 116711.
- [39] C. Shi, A.Y. Zhou, D.L. Fang, T. Lu, J.Y. Wang, Y.X. Song, L. Lyu, W.L. Wu, C.B. Huang, W.L. Li, Oregano essential oil/ $\beta$ -cyclodextrin inclusion compound polylactic acid/polycaprolactone electrospun nanofibers for active food packaging, *Chem. Eng. J.* 445 (2022) 136746.
- [40] W.X. Cao, D. Xia, L.X. Zhou, Y. Liu, D.H. Wang, C.Y. Liang, M.L. Chen, Antibacterial and antioxidant wound dressings with pH responsive release properties accelerate chronic wound healing, *Mater. Today Phys.* 40 (2024) 101316.
- [41] P. Gong, L.L. Ren, X.H. Gao, J. Long, W.D. Tian, M. He, A novel barrier membrane with long-term ROS scavenging function for complete prevention of postoperative adhesion, *Mater. Design* 238 (2024) 112691.
- [42] K. Jiao, M.L. Sun, W.Y. Jia, Y. Liu, S.R. Wang, Y.H. Yang, Z.H. Dai, L.P. Liu, Z.Q. Cheng, G.M. Liu, Y.G. Luo, The polycaprolactone and silk fibroin nanofibers with Janus-structured sheaths for antibacterial and antioxidant by loading Taxifolin, *Heliyon* 10 (2024) e33770.
- [43] E.A. Abdulhameed, K.G.A. Rani, F.M. AlGhalban, E.A. Abou Neel, N. Khalifa, K.A. Khalil, M. Omar, A. Samsudin, Managing oxidative stress using vitamin C to improve biocompatibility of polycaprolactone for bone regeneration in vitro, *ACS Omega* 9 (2024) 31776–31788.
- [44] Y.Z. Wang, X.Z. Wang, D. Zhou, X. Xia, H.M. Zhou, Y. Wang, H.Z. Ke, Preparation and characterization of polycaprolactone (PCL) antimicrobial wound dressing loaded with pomegranate peel extract, *ACS Omega* 8 (2023) 20323–20331.
- [45] R.M. Liang, J.M. Zhao, B. Li, P.A. Cai, X.J. Loh, C.H. Xu, P. Chen, D. Kai, L. Zheng, Implantable and degradable antioxidant poly( $\epsilon$ -caprolactone)-lignin nanofiber membrane for effective osteoarthritis treatment, *Biomaterials* 230 (2020) 119601.
- [46] D. Senanayake, P. Yapa, S. Sabare, I. Munaweera, M.M. Weerasekera, T.N.B. Etampawala, M. Sethunga, D. Attygalle, S. Amarasinghe, Combined antimicrobial and anti-inflammatory properties of electrospun PCL nanohybrids infused with metal-turmeric oleoresin and metalcurcuminoids, *RSC Adv.* 15 (2025) 20061–20083.
- [47] H.A. Rather, R. Thakore, R. Singh, D. Jhala, S. Singh, R. Vasita, Antioxidative study of cerium oxide nanoparticle functionalised PCL-gelatin electrospun fibers for wound healing application, *Bioact. Mater.* 3 (2018) 201–211.
- [48] F. Wu, Y.R. Wang, Y.F. Li, L.Q. Shi, L. Yuan, Y.J. Ren, H.C. van der Mei, Y. Liu, Single-atom Cu anchored on carbon nitride as a bifunctional glucose oxidase and peroxidase nanozyme for antibacterial therapy, *ACS Nano* 19 (2025) 10816–10828.
- [49] C. Beaucham, I. Fridovich, Superoxide dismutase - improved assays and an assay applicable to acrylamide gels, *Anal. Biochem.* 44 (1971) 276–287.
- [50] P.L. Zhou, H.B. Yu, W.H. Zou, Z.D. Wang, L.Q. Liu, High-resolution and controllable nanodeposition pattern of Ag nanoparticles by electrohydrodynamic jet printing combined with coffee ring effect, *Adv. Mater. Interfaces* 6 (2019) 1900912.
- [51] V.R. Dugyala, M.G. Basavaraj, Evaporation of sessile drops containing colloidal rods: Coffee-ring and order-disorder transition, *J. Phys. Chem. B* 119 (2015) 3860–3867.
- [52] A.N. Pstryakov, V.P. Petranovskii, A. Kryazhov, O. Ozhereliev, N. Pfänder, A. Knop-Gericke, Study of copper nanoparticles formation on supports of different nature by UV-Vis diffuse reflectance spectroscopy, *Chem. Phys. Lett.* 385 (2004) 173–176.
- [53] C. Baptista, A. Azagury, H. Shin, C.M. Baker, E. Ly, R. Lee, E. Mathiowitz, The effect of temperature and pressure on polycaprolactone morphology, *Polymer* 191 (2020) 122227.
- [54] R. Yaseri, M. Fadaie, E. Mirzaei, H. Samadian, A. Ebrahimezhad, Surface modification of polycaprolactone nanofibers through hydrolysis and aminolysis: a comparative study on structural characteristics, mechanical properties, and cellular performance, *Sci. Rep.* 13 (2023) 9434.
- [55] T.G. Halmagyi, A. Voros, S. Saringer, V. Hornok, N.V. May, G.F. Samu, I. Szenti, A. Szerlauth, Z. Konya, I. Szilágyi, Coamplified nanozyme cocktails for cascade reaction-driven antioxidant treatments, *ACS Appl. Mater. Interfaces* 16 (2024) 54485–54495.